

# Flavour Separation of Helicity Distributions from Deep Inelastic Muon–Deuteron Scattering

*COMPASS Collaboration*

## Abstract

We present a LO evaluation of helicity densities of valence,  $\Delta u_v + \Delta d_v$ , non-strange sea,  $\Delta \bar{u} + \Delta \bar{d}$ , and strange quarks,  $\Delta s$  (assumed to be equal to  $\Delta \bar{s}$ ). They have been obtained from the inclusive asymmetry  $A_{1,d}$  and the semi-inclusive asymmetries  $A_{1,d}^{\pi^+}$ ,  $A_{1,d}^{\pi^-}$ ,  $A_{1,d}^{K^+}$ ,  $A_{1,d}^{K^-}$  measured in polarised deep inelastic muon-deuteron scattering. The full deuteron statistics of COMPASS (years 2002–2004 and 2006) has been used. The data cover the range  $Q^2 > 1 \text{ (GeV/c)}^2$  and  $0.004 < x < 0.3$ . Both non-strange densities are found to be in a good agreement with previous measurements. The distribution of  $\Delta s(x)$  is compatible with zero in the whole measured range, in contrast to the shape of the strange quark helicity distribution obtained in most LO and NLO QCD fits. The sensitivity of the values of  $\Delta s(x)$  upon the choice of fragmentation functions used in the derivation is discussed.

Keywords: COMPASS; double-spin asymmetry; helicity density; parton distribution function; flavour separation analysis; polarised DIS and SIDIS reactions; charged kaon asymmetry

PACS: 13.60.Hb, 13.60.Le, 13.88+e

## COMPASS Collaboration

M. Alekseev<sup>30</sup>, V.Yu. Alexakhin<sup>8</sup>, Yu. Alexandrov<sup>16</sup>, G.D. Alexeev<sup>8</sup>, A. Amoroso<sup>28</sup>, A. Austregisilio<sup>11,18</sup>, B. Badelek<sup>31</sup>, F. Balestra<sup>28</sup>, J. Ball<sup>23</sup>, J. Barth<sup>4</sup>, G. Baum<sup>1</sup>, Y. Bedfer<sup>23</sup>, J. Bernhard<sup>14</sup>, R. Bertini<sup>28</sup>, M. Bettinelli<sup>17</sup>, R. Birsa<sup>25</sup>, J. Bisplinghoff<sup>3</sup>, P. Bordalo<sup>13,a</sup>, F. Bradamante<sup>26</sup>, A. Bravar<sup>25</sup>, A. Bressan<sup>26</sup>, G. Brona<sup>31</sup>, E. Burtin<sup>23</sup>, M.P. Busa<sup>28</sup>, A. Chapiro<sup>27</sup>, M. Chiosso<sup>28</sup>, S.U. Chung<sup>18</sup>, A. Ciuttin<sup>25,27</sup>, M. Colantoni<sup>29</sup>, M.L. Crespo<sup>25,27</sup>, S. Dalla Torre<sup>25</sup>, T. Dafni<sup>23</sup>, S. Das<sup>7</sup>, S.S. Dasgupta<sup>6</sup>, O.Yu. Denisov<sup>29,b</sup>, L. Dhara<sup>7</sup>, V. Diaz<sup>25,27</sup>, A.M. Dinkelbach<sup>18</sup>, S.V. Donskov<sup>22</sup>, N. Doshita<sup>2,33</sup>, V. Duic<sup>26</sup>, W. Dünneweber<sup>17</sup>, A. Efremov<sup>8</sup>, A. El Alaoui<sup>23</sup>, P.D. Eversheim<sup>3</sup>, W. Eyrich<sup>9</sup>, M. Faessler<sup>17</sup>, A. Ferrero<sup>28,11</sup>, M. Finger<sup>20</sup>, M. Finger jr.<sup>8</sup>, H. Fischer<sup>10</sup>, C. Franco<sup>13</sup>, J.M. Friedrich<sup>18</sup>, R. Garfagnini<sup>28</sup>, F. Gautheron<sup>1</sup>, O.P. Gavrichtchouk<sup>8</sup>, R. Gazda<sup>31</sup>, S. Gerassimov<sup>16,18</sup>, R. Geyer<sup>17</sup>, M. Giorgi<sup>26</sup>, B. Gobbo<sup>25</sup>, S. Goertz<sup>2,4</sup>, S. Grabmüller<sup>18</sup>, O.A. Grajek<sup>31</sup>, A. Grasso<sup>28</sup>, B. Grube<sup>18</sup>, R. Gushterski<sup>8</sup>, A. Guskov<sup>8</sup>, F. Haas<sup>18</sup>, R. Hagemann<sup>10</sup>, D. von Harrach<sup>14</sup>, T. Hasegawa<sup>15</sup>, J. Heckmann<sup>2</sup>, F.H. Heinsius<sup>10</sup>, R. Hermann<sup>14</sup>, F. Herrmann<sup>10</sup>, C. Heß<sup>2</sup>, F. Hinterberger<sup>3</sup>, N. Horikawa<sup>19,c</sup>, Ch. Höppner<sup>18</sup>, N. d'Hose<sup>23</sup>, C. Ilgner<sup>11,17</sup>, S. Ishimoto<sup>19,d</sup>, O. Ivanov<sup>8</sup>, Yu. Ivanshin<sup>8</sup>, T. Iwata<sup>33</sup>, R. Jahn<sup>3</sup>, P. Jasinski<sup>14</sup>, G. Jegou<sup>23</sup>, R. Joosten<sup>3</sup>, E. Kabuß<sup>14</sup>, W. Käfer<sup>10</sup>, D. Kang<sup>10</sup>, B. Ketzer<sup>18</sup>, G.V. Khaustov<sup>22</sup>, Yu.A. Khokhlov<sup>22</sup>, J. Kiefer<sup>10</sup>, Yu. Kisselev<sup>1,2</sup>, F. Klein<sup>4</sup>, K. Klimaszewski<sup>31</sup>, S. Koblitz<sup>14</sup>, J.H. Koivuniemi<sup>2</sup>, V.N. Kolosov<sup>22</sup>, E.V. Komissarov<sup>8,+</sup>, K. Kondo<sup>2,33</sup>, K. Königsmann<sup>10</sup>, R. Konopka<sup>18</sup>, I. Konorov<sup>16,18</sup>, V.F. Konstantinov<sup>22</sup>, A. Korzenev<sup>14,b</sup>, A.M. Kotzinian<sup>8,23</sup>, O. Kouznetsov<sup>8,23</sup>, K. Kowalik<sup>31,23</sup>, M. Krämer<sup>18</sup>, A. Kral<sup>21</sup>, Z.V. Kroumchtein<sup>8</sup>, R. Kuhn<sup>18</sup>, F. Kunne<sup>23</sup>, K. Kurek<sup>31</sup>, J.M. Le Goff<sup>23</sup>, A.A. Lednev<sup>22</sup>, A. Lehmann<sup>9</sup>, S. Levorato<sup>26</sup>, J. Lichtenstadt<sup>24</sup>, T. Liska<sup>21</sup>, A. Maggiora<sup>29</sup>, M. Maggiora<sup>28</sup>, A. Magnon<sup>23</sup>, G.K. Mallot<sup>11</sup>, A. Mann<sup>18</sup>, C. Marchand<sup>23</sup>, J. Marroncle<sup>23</sup>, A. Martin<sup>26</sup>, J. Marzec<sup>32</sup>, F. Massmann<sup>3</sup>, T. Matsuda<sup>15</sup>, A.N. Maximov<sup>8,+</sup>, W. Meyer<sup>2</sup>, T. Michigami<sup>33</sup>, Yu.V. Mikhailov<sup>22</sup>, M.A. Moinester<sup>24</sup>, A. Mutter<sup>10,14</sup>, A. Nagaytsev<sup>8</sup>, T. Nagel<sup>18</sup>, J. Nassalski<sup>31</sup>, S. Negrini<sup>3</sup>, F. Nerling<sup>10</sup>, S. Neubert<sup>18</sup>, D. Neyret<sup>23</sup>, V.I. Nikolaenko<sup>22</sup>, A.G. Olshevsky<sup>8</sup>, M. Ostrick<sup>4,14</sup>, A. Padee<sup>32</sup>, R. Panknin<sup>4</sup>, D. Panzieri<sup>30</sup>, B. Parsamyan<sup>28</sup>, S. Paul<sup>18</sup>, B. Pawlukiewicz-Kaminska<sup>31</sup>, E. Perevalova<sup>8</sup>, G. Pesaro<sup>26</sup>, D.V. Peshekhonov<sup>8</sup>, G. Piragino<sup>28</sup>, S. Platchkov<sup>23</sup>, J. Pochodzalla<sup>14</sup>, J. Polak<sup>12,26</sup>, V.A. Polyakov<sup>22</sup>, G. Pontecorvo<sup>8</sup>, J. Pretz<sup>4</sup>, C. Quintans<sup>13</sup>, J.-F. Rajotte<sup>17</sup>, S. Ramos<sup>13,a</sup>, V. Rapatsky<sup>8</sup>, G. Reicherz<sup>2</sup>, D. Reggiani<sup>11</sup>, A. Richter<sup>9</sup>, F. Robinet<sup>23</sup>, E. Rocco<sup>28</sup>, E. Rondio<sup>31</sup>, D.I. Ryabchikov<sup>22</sup>, V.D. Samoylenko<sup>22</sup>, A. Sandacz<sup>31</sup>, H. Santos<sup>13,a</sup>, M.G. Sapozhnikov<sup>8</sup>, S. Sarkar<sup>7</sup>, I.A. Savin<sup>8</sup>, G. Sbrizza<sup>26</sup>, P. Schiavon<sup>26</sup>, C. Schill<sup>10</sup>, L. Schmitt<sup>18,e</sup>, W. Schröder<sup>9</sup>, O.Yu. Shevchenko<sup>8</sup>, H.-W. Siebert<sup>14</sup>, L. Silva<sup>13</sup>, L. Sinha<sup>7</sup>, A.N. Sissakian<sup>8</sup>, M. Slunicka<sup>8</sup>, G.I. Smirnov<sup>8</sup>, S. Sosio<sup>28</sup>, F. Sozzi<sup>26</sup>, A. Srnka<sup>5</sup>, M. Stolarski<sup>31,11</sup>, M. Sulc<sup>12</sup>, R. Sulej<sup>32</sup>, S. Takekawa<sup>26</sup>, S. Tessaro<sup>25</sup>, F. Tessarotto<sup>25</sup>, A. Teufel<sup>9</sup>, L.G. Tkatchev<sup>8</sup>, G. Venugopal<sup>3</sup>, M. Virius<sup>21</sup>, N.V. Vlassov<sup>8</sup>, A. Vossen<sup>10</sup>, Q. Weitzel<sup>18</sup>, K. Wenzl<sup>10</sup>, R. Windmolders<sup>4</sup>, W. Wislicki<sup>31</sup>, H. Wollny<sup>10</sup>, K. Zarembo<sup>32</sup>, M. Zavertyaev<sup>16</sup>, E. Zemlyanichkina<sup>8</sup>, M. Ziembicki<sup>32</sup>, J. Zhao<sup>14,25</sup>, N. Zhuravlev<sup>8</sup> and A. Zvyagin<sup>17</sup>

- 
- 1) Universität Bielefeld, Fakultät für Physik, 33501 Bielefeld, Germany<sup>f)</sup>
  - 2) Universität Bochum, Institut für Experimentalphysik, 44780 Bochum, Germany<sup>f)</sup>
  - 3) Universität Bonn, Helmholtz-Institut für Strahlen- und Kernphysik, 53115 Bonn, Germany<sup>f)</sup>
  - 4) Universität Bonn, Physikalisches Institut, 53115 Bonn, Germany<sup>f)</sup>
  - 5) Institute of Scientific Instruments, AS CR, 61264 Brno, Czech Republic<sup>g)</sup>
  - 6) Burdwan University, Burdwan 713104, India<sup>h)</sup>
  - 7) Matrivani Institute of Experimental Research & Education, Calcutta-700 030, India<sup>i)</sup>
  - 8) Joint Institute for Nuclear Research, 141980 Dubna, Moscow region, Russia
  - 9) Universität Erlangen–Nürnberg, Physikalisches Institut, 91054 Erlangen, Germany<sup>f)</sup>
  - 10) Universität Freiburg, Physikalisches Institut, 79104 Freiburg, Germany<sup>f)</sup>
  - 11) CERN, 1211 Geneva 23, Switzerland
  - 12) Technical University in Liberec, 46117 Liberec, Czech Republic<sup>g)</sup>
  - 13) LIP, 1000-149 Lisbon, Portugal<sup>j)</sup>
  - 14) Universität Mainz, Institut für Kernphysik, 55099 Mainz, Germany<sup>f)</sup>
  - 15) University of Miyazaki, Miyazaki 889-2192, Japan<sup>k)</sup>
  - 16) Lebedev Physical Institute, 119991 Moscow, Russia
  - 17) Ludwig-Maximilians-Universität München, Department für Physik, 80799 Munich, Germany<sup>f, l)</sup>
  - 18) Technische Universität München, Physik Department, 85748 Garching, Germany<sup>f, l)</sup>
  - 19) Nagoya University, 464 Nagoya, Japan<sup>k)</sup>
  - 20) Charles University, Faculty of Mathematics and Physics, 18000 Prague, Czech Republic<sup>g)</sup>
  - 21) Czech Technical University in Prague, 16636 Prague, Czech Republic<sup>g)</sup>
  - 22) State Research Center of the Russian Federation, Institute for High Energy Physics, 142281 Protvino, Russia
  - 23) CEA DAPNIA/SPhN Saclay, 91191 Gif-sur-Yvette, France
  - 24) Tel Aviv University, School of Physics and Astronomy, 69978 Tel Aviv, Israel<sup>m)</sup>
  - 25) Trieste Section of INFN, 34127 Trieste, Italy
  - 26) University of Trieste, Department of Physics and Trieste Section of INFN, 34127 Trieste, Italy
  - 27) Abdus Salam ICTP and Trieste Section of INFN, 34127 Trieste, Italy
  - 28) University of Turin, Department of Physics and Torino Section of INFN, 10125 Turin, Italy
  - 29) Torino Section of INFN, 10125 Turin, Italy
  - 30) University of Eastern Piedmont, 1500 Alessandria, and Torino Section of INFN, 10125 Turin, Italy
  - 31) Sołtan Institute for Nuclear Studies and University of Warsaw, 00-681 Warsaw, Poland<sup>n)</sup>
  - 32) Warsaw University of Technology, Institute of Radioelectronics, 00-665 Warsaw, Poland<sup>o)</sup>
  - 33) Yamagata University, Yamagata, 992-8510 Japan<sup>k)</sup>
- + ) Deceased
- a) Also at IST, Universidade Técnica de Lisboa, Lisbon, Portugal
  - b) On leave of absence from JINR Dubna
  - c) Also at Chubu University, Kasugai, Aichi, 487-8501 Japan<sup>j)</sup>
  - d) Also at KEK, 1-1 Oho, Tsukuba, Ibaraki, 305-0801 Japan
  - e) Also at GSI mbH, Planckstr. 1, D-64291 Darmstadt, Germany
  - f) Supported by the German Bundesministerium für Bildung und Forschung
  - g) Supported by Czech Republic MEYS grants ME492 and LA242
  - h) Supported by DST-FIST II grants, Govt. of India
  - i) Supported by the Shailabala Biswas Education Trust
  - j) Supported by the Portuguese FCT - Fundação para a Ciência e Tecnologia grants POCTI/FNU/49501/2002 and POCTI/FNU/50192/2003
  - k) Supported by the MEXT and the JSPS under the Grants No.18002006, No.20540299 and No.18540281; Daiko Foundation and Yamada Foundation
  - l) Supported by the DFG cluster of excellence ‘Origin and Structure of the Universe’ ([www.universe-cluster.de](http://www.universe-cluster.de))
  - m) Supported by the Israel Science Foundation, founded by the Israel Academy of Sciences and Humanities
  - n) Supported by Ministry of Science and Higher Education grant 41/N-CERN/2007/0
  - o) Supported by KBN grant nr 134/E-365/SPUB-M/CERN/P-03/DZ299/2000

## 1 Introduction

Among the various sea quarks contributing to the nucleon spin, the strange quark is the only one accessible in inclusive lepton-nucleon scattering experiments. The first moment of the strange quark helicity distribution,  $\Delta s + \Delta \bar{s}$ , has been found to be negative already twenty years ago in the EMC experiment [1] under the assumption of  $SU(3)_F$  symmetry in hyperon  $\beta$  decays. This result has been confirmed with improved precision by recent measurements performed by HERMES [2] and by COMPASS which has obtained

$$\Delta s + \Delta \bar{s} = -0.09 \pm 0.01(\text{stat.}) \pm 0.02(\text{syst.}) \quad (1)$$

at  $Q^2 = 10(\text{GeV}/c)^2$  at leading order (LO) in QCD [3]. Inclusive experiments, however, provide an evaluation of the first moment  $\Delta s + \Delta \bar{s}$  only. The shape as a function of the Bjorken scaling variable  $x$  is determined in global fits of the nucleon spin structure function  $g_1(x, Q^2)$  where a parameterisation of the strange quark helicity as a function of  $x$  assumed to be valid at some reference value of the photon virtuality,  $Q_0^2$ , is evolved to the  $Q^2$  of each data point and fitted to the measured values. The resulting distribution  $\Delta s(x)$ , further assumed to be equal to  $\Delta \bar{s}(x)$ , is generally concentrated at the highest values of  $x$  compatible with the positivity limit  $|\Delta s(x, Q^2)| \leq s(x, Q^2)$  [4, 5].

Direct information on the distribution  $\Delta s(x)$  can be obtained from semi-inclusive channels, in which interactions on strange quarks are enhanced, such as charged kaon production. These measurements, which require final state particle identification, became only feasible in recent experiments and the only results published so far are from the HERMES experiment [6, 7, 8].

In a full flavour decomposition analysis, the HERMES collaboration has obtained  $\Delta s = 0.028 \pm 0.033(\text{stat.}) \pm 0.009(\text{syst.})$  in the range  $0.023 < x < 0.6$  [7]. In their most recent analysis of the charged kaon and inclusive asymmetries in deuteron data, they have obtained  $\Delta s + \Delta \bar{s} = 0.037 \pm 0.019(\text{stat.}) \pm 0.027(\text{syst.})$  [8]. The negative values of  $\Delta s(x)$  expected from the full first moment have thus never been observed in the  $x$  range covered by HERMES. The implication of a positive  $\Delta s$  in a limited experimental range was discussed in relation with the assumed  $SU(3)$  flavour symmetry and it was shown that a non-negative first moment of  $\Delta s$  was highly unlikely [9]. This situation is clearly reflected in the result of a global fit including all inclusive and semi-inclusive results in the DIS region: the fitted distribution of  $\Delta s(x)$  which is positive at  $x > 0.03$  receives a negative contribution in the unmeasured low  $x$  range, to bring its first moment close to the values of Eq. (1) [10].

In this paper we present a new precise measurement of the inclusive and semi-inclusive double spin asymmetries measured on an isoscalar target by the COMPASS experiment at CERN and a LO evaluation of the polarised parton distributions  $\Delta u_v + \Delta d_v$ ,  $\Delta \bar{u} + \Delta \bar{d}$  and  $\Delta s (= \Delta \bar{s})$ .

At LO in QCD under the assumption of independent quark fragmentation, the double spin asymmetries for hadrons  $h$  produced in the current fragmentation region can be decomposed into a sum of products of quark helicity distributions  $\Delta q(x, Q^2)$  times quark fragmentation functions  $D_q^h(z, Q^2)$  where  $z$  is the fraction of the virtual photon energy taken by the hadron  $h$ :

$$A_1^h(x, Q^2, z) = \frac{\sum_q e_q^2 \Delta q(x, Q^2) D_q^h(z, Q^2)}{\sum_q e_q^2 q(x, Q^2) D_q^h(z, Q^2)}. \quad (2)$$

A previous determination of the quark helicity distributions performed by SMC [11] covers a kinematic range similar to the COMPASS data but does not provide a determination of  $\Delta s$  due to the lack of hadron identification.

The deuteron data presented in this paper were collected in the years 2002-2004 and 2006. The produced hadrons cover a large phase space. In the present analysis only those identified as pions or kaons are used.

## 2 Experimental setup

A general description of the COMPASS spectrometer in the initial configuration is given in [12]. Only modifications introduced after the year 2005 will be mentioned here. They mainly concern the polarised target, the large area trackers around the first spectrometer magnet (SM1), and the RICH detector.

Before 2005 the target solenoid magnet was the one previously used by the SMC experiment [13] with an aperture of  $\pm 70$  mrad as seen from the upstream end of the target. The new solenoid magnet [14] installed in 2005 has an acceptance of  $\pm 180$  mrad. Before 2005 the polarised target, located inside the solenoid, consisted of two cells, each 60 cm long and 3 cm in diameter, separated by 10 cm. A three cell target has been installed in the new magnet. In this configuration the central cell is 60 cm long and the two outer ones 30 cm long, separated by 5 cm. The total amount of material thus remains unchanged.

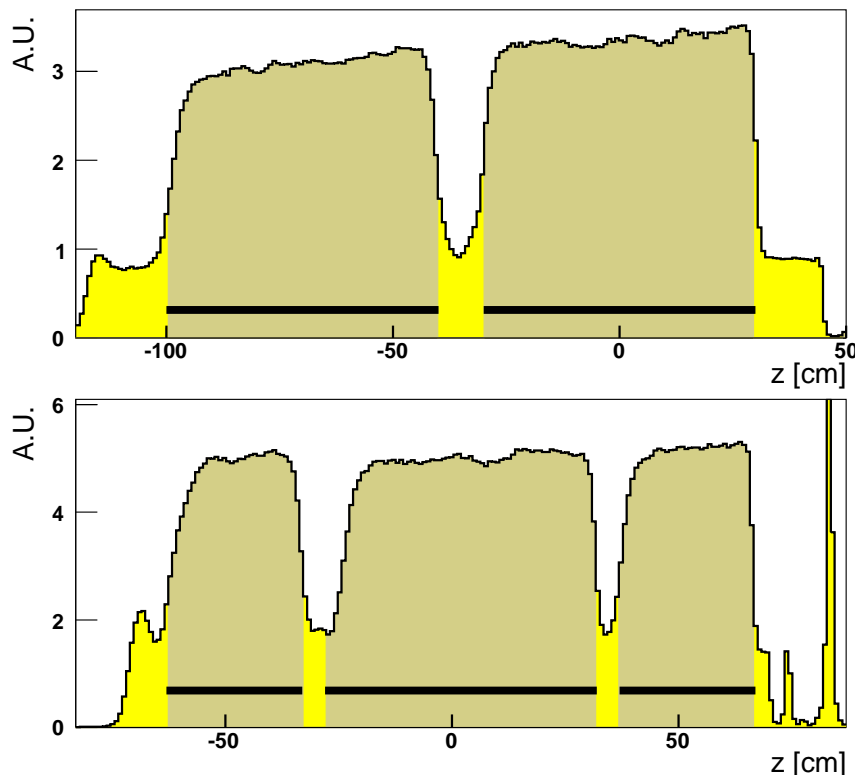


Figure 1: Distribution of the interaction vertices along the beam axis for the 2 cell (years 2002–2004) and 3 cell (year 2006) target configurations. The solid lines show the length of the cells.

The distribution of the interaction vertices along the beam axis for the events used in the present analysis is shown in Fig. 1 for the old and new target configurations.

The deuterated lithium target material ( ${}^6\text{LiD}$ ) is longitudinally polarised with the method of dynamic nuclear polarisation (DNP) [15]. In the old as well as in the new configuration neighbouring cells of the targets are polarised in opposite directions so that data from both spin directions are recorded at the same time. The absolute value of the averaged polarisation varies between 0.50 and 0.56. Before 2005 the spin directions in the target cells were reversed every 8 hours by rotating the magnetic field direction. In this way, fluxes and acceptances cancel out in the calculation of spin asymmetries, provided that the ratio of acceptances remains unchanged after spin reversal. In the new configuration, the data samples obtained with both spin orientations have in average the same acceptance, which limits false asymmetries. In view of this, the magnetic field direction was rotated only once per day during the 2006 data taking. In order to minimise possible acceptance effects related to the orientation of the solenoid field, the sign of the polarisation in each target cell was also reversed a few times per year by changing the DNP microwave frequencies.

Several modifications have been introduced in the tracking detectors around SM1 in order to match the enlarged acceptance of the new solenoid: an additional medium size drift chamber station (DC) has been installed upstream of SM1 and two smaller DCs, downstream of SM1, have been replaced by a new larger one and by a straw tube station.

A major upgrade has also been applied to the RICH detector to improve its performance in terms of efficiency and purity [16]: in the most critical central region, photon detection previously provided by large-size MWPCs with CsI photocathodes has been replaced by a system based on multi-anode PMTs. It improves considerably the signal-to-noise ratio in the region where the beam halo is largest. In addition the readout system for the peripheral region has been replaced by a faster one.

### 3 Asymmetries

All events used in the present analysis are required to have a reconstructed primary interaction vertex defined initially by the incoming and the scattered muon trajectories (the reconstruction procedure is described in Ref.[17]). The energy of the beam muon is constrained to be in the interval  $140 < E_\mu < 180$  GeV. To equalise fluxes through the different target cells, it is required for the trajectory of the incoming muon to cross entirely all cells. This condition is essential because it allows to cancel out the muon flux in

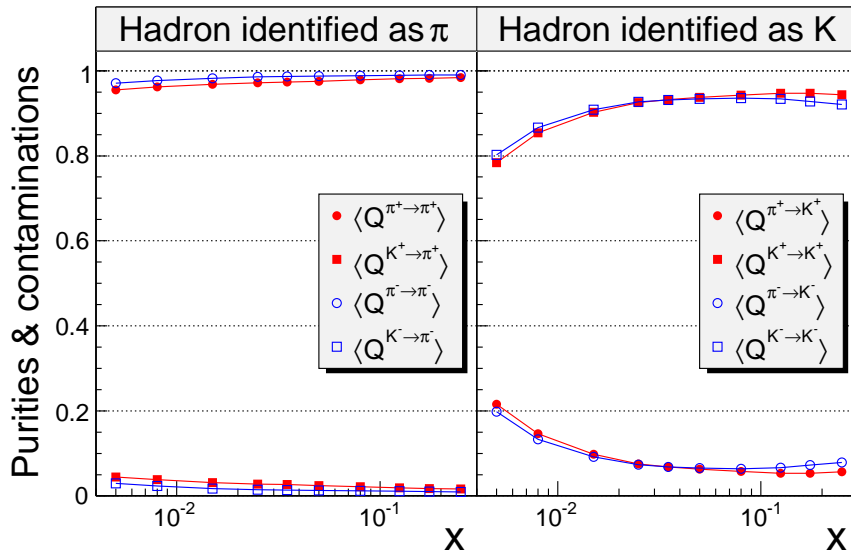


Figure 2: Purities  $Q^{\pi \rightarrow \pi}$ ,  $Q^{K \rightarrow K}$  and contaminations  $Q^{\pi \rightarrow K}$ ,  $Q^{K \rightarrow \pi}$  calculated for the 2004 data.

the calculation of asymmetries. The kinematic region is defined by cuts on the photon virtuality,  $Q^2$ , and the fractional energy,  $y$ , transferred from the beam muon to the virtual photon. DIS events are selected by requiring  $Q^2 > 1$  ( $\text{GeV}/c$ )<sup>2</sup>. The requirement  $y > 0.1$  removes events affected by bad resolution and low photon polarisation. The region most affected by radiative corrections is eliminated by the cut  $y < 0.9$ .

The  $x$  range covered in the present analysis extends from 0.004 to 0.3. The low limit is defined by the kinematical cut  $Q^2 > 1$  ( $\text{GeV}/c$ )<sup>2</sup>. The upper limit is set to  $x = 0.3$  because interactions on sea quarks are negligible at higher  $x$ . The total energy of the  $\gamma^*$ -nucleon system in the selected events covers the range  $5 \lesssim W \lesssim 17$  GeV. The statistics of 135.1 million events includes the sample used in Ref.[4] and reduces the statistical errors by about 30 %.

Hadron tracks are required to originate from the main vertex. A cut on the fractional energy  $z > 0.2$  is applied to the hadron candidates in order to select those produced in the current fragmentation region. In addition an upper limit  $z < 0.85$  is imposed in order to suppress hadrons from diffractive processes and to avoid contamination from wrongly identified muons. Several other cuts are applied to guarantee the quality of the selected track sample: the first reconstructed track point must be upstream of SM1; tracks reconstructed only upstream of SM1 are rejected and those crossing more than 30 radiation lengths of material are not accepted as hadrons.

Hadron identification is performed using the RICH detector. For the present analysis, the momenta of hadrons are restricted to the range common to pion and kaon identification  $10 < p < 50$  GeV/ $c$ . The expected distributions of photo-electrons are calculated for different particle masses as well as for the background assumption. These distributions are compared to the observed one and the mass is assigned according to the ratios of their likelihoods. The statistics available for the  $\pi^+$  ( $\pi^-$ ) and  $K^+$  ( $K^-$ ) samples after all cuts is 22.8(20.5), and 4.8(3.3) millions, respectively.

Since the samples of identified pions and kaons do not fully correspond to the true ones, an unfolding procedure must be applied to correct rates and asymmetries. In a first step, the elements of the identification efficiency matrix,  $P^{t \rightarrow i}$ , are calculated. They represent the probability for a particle of true type  $t$  to be identified as type  $i$ . The values of  $P^{t \rightarrow i}$  are obtained from samples of reconstructed pions and kaons resulting from  $K_S^0$  and  $\phi$  decays, respectively. Since the RICH performance depends critically on the phase space of particles, the elements  $P^{t \rightarrow i}$  are calculated in bins of momentum and polar angle (angle w.r.t. beam axis) of the selected particle.

In a second step the contributions,  $Q^{t \rightarrow i}$ , from different hadron species  $t$  to the identified sample  $i$  are determined. They depend not only on the identification efficiencies  $P^{t \rightarrow i}$  but also on the observed hadron rates and therefore must be calculated separately for every bin of  $x$ . As an example the contributions  $Q^{\pi \rightarrow \pi}$ ,  $Q^{K \rightarrow K}$  (called "purities") and  $Q^{\pi \rightarrow K}$ ,  $Q^{K \rightarrow \pi}$  (called "contaminations") for positive and negative hadrons in the 2004 data are shown in Fig. 2 as a function of  $x$ . In general,  $Q^{\pi \rightarrow \pi}$  is close to 1.0 and  $Q^{K \rightarrow K}$  varies from about 0.8 at low  $x$  to about 0.93 at medium  $x$ . In view of this, unfolding can only have a significant effect at low  $x$  but since the pion and kaon asymmetries are similar in this region, its effect remains small as compared to the statistical errors.

The inclusive asymmetries and the unfolded hadron asymmetries have been corrected for radiative

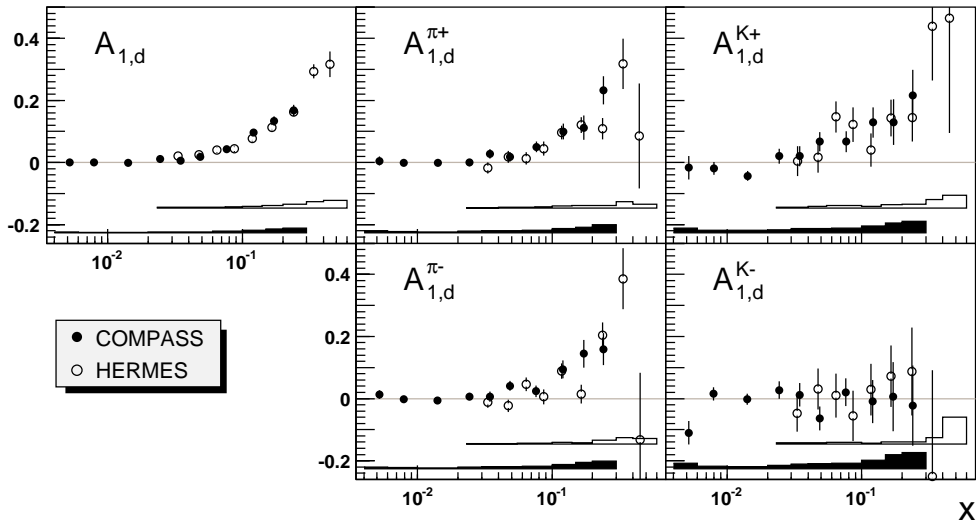


Figure 3: Comparison of final asymmetries of COMPASS as a function of  $x$  with results of HERMES [7]. Bands at bottom of graphs represent systematic uncertainties. Solid markers and bands correspond to COMPASS data. Open markers and bands are taken from the HERMES publication.

effects according to the procedure of Ref.[18] and are shown in Fig. 3 as a function of  $x$ . The values of the inclusive asymmetry are in good agreement with those of Ref.[4]. The results of HERMES, the only other experiment which measured asymmetries of identified hadrons [7], are shown for comparison. The two sets of measurements are well compatible and in the region of kinematic overlap the statistical precision of the two experiments is generally comparable. However COMPASS extends the measured region towards  $x = 0$  by an order of magnitude. It is also observed that all asymmetries, except  $A_{1,d}^{K^-}$ , are quite similar to each other. This feature is expected due to the isoscalar symmetry of the  ${}^6\text{LiD}$  target. The  $K^-$  asymmetry is consistent with zero over the full range of  $x$ . The values of the inclusive and semi-inclusive asymmetries are listed with their statistical and systematic errors in Tables 2 and 3. Correlations between different asymmetries in bins of  $x$  are listed in Table 4.

There are several sources of systematic uncertainties in the determination of the asymmetries. The error of the target polarisation measurement and the error on the parameterisation of the beam polarisation amount to 5% of their respective value. The uncertainty related to the dilution factor, which includes the dilution due to radiative events on the deuteron, is 2% over the full range of  $x$ . The ratio  $R = \sigma^L/\sigma^T$  used to calculate the depolarisation factor [19] gives an error of 2-3%. When added in quadrature these multiplicative uncertainties amount to a systematic error of 8% of the asymmetry. The systematic error also accounts for false asymmetries which could be generated by instabilities in some components of the spectrometer. Asymmetries due to apparatus effects have been searched for in combinations of data samples where the physical asymmetry cancels out. The asymmetries observed in these combinations were found compatible with zero. Systematic effects have also been studied by comparing results obtained with different microwave settings. No significant difference was found. The possible error due to false asymmetries was evaluated as a fraction of the statistical error:  $\sigma_{syst} < 0.4 \sigma_{stat}$ [4]. The total systematic uncertainty is shown by the bands at the bottom of each plot in Fig. 3.

#### 4 Polarised PDFs from a fit to the asymmetries

As in our previous LO analysis [3], we assumed that hadrons in the current fragmentation region are produced by independent quark fragmentation, so that their spin asymmetries can be written in terms of parton distribution functions ( $q(x, Q^2)$ ,  $\Delta q(x, Q^2)$ ) and fragmentation functions (FFs)  $D_q^h(z, Q^2)$  according to Eq. (2). In the present analysis we use the unpolarised parton distribution functions (PDFs) from MRST [20]<sup>1)</sup> and the recent DSS parameterisation of FFs at LO which was obtained from a combined analysis of inclusive pion and kaon production data from  $e^+e^-$  annihilation, semi-inclusive DIS data ("SIDIS") from HERMES and proton-proton collider data [21]. In order to test the dependence of the polarised PDFs on the FFs, we also show the values obtained with the EMC FFs [22]. In contrast to other parameterisations which are derived from global fits, the latter ones have been extracted from the EMC data only, so that only non-strange quark fragmentation could be measured. Therefore, in addition

<sup>1)</sup> We use the LO set with three quark flavours.

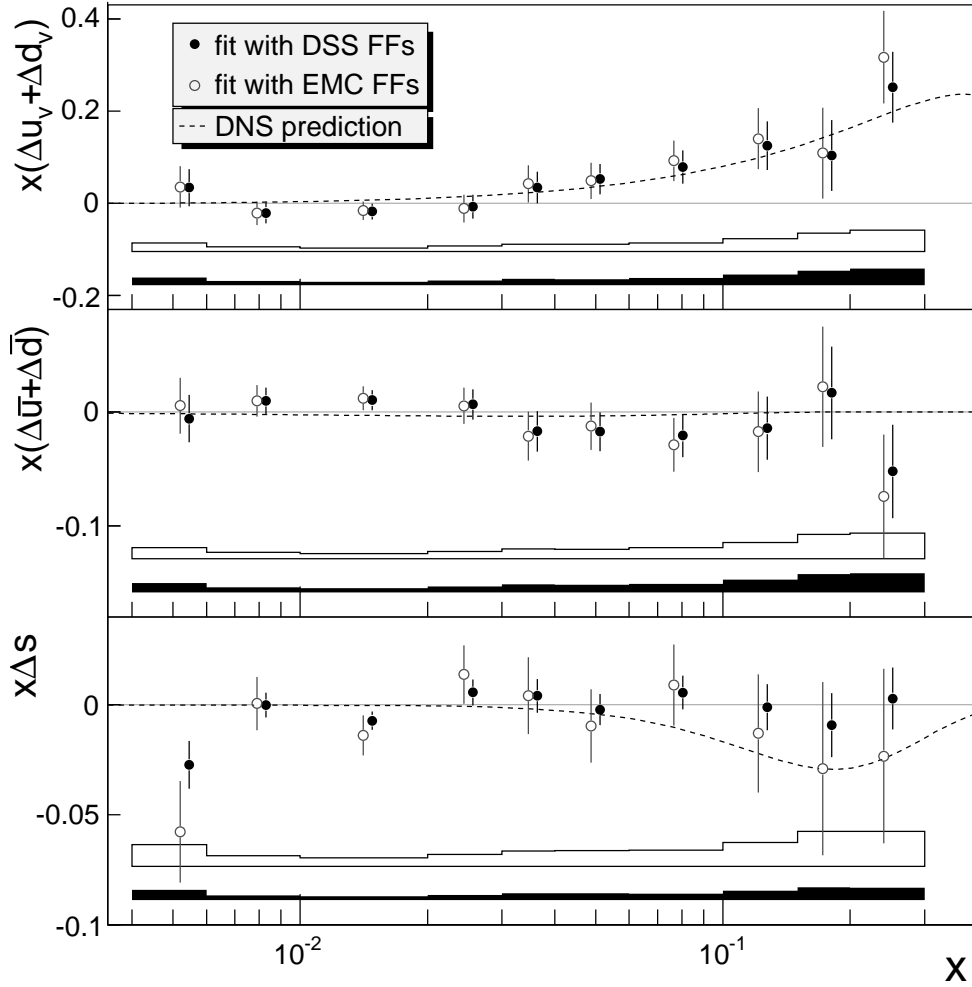


Figure 4: The quark helicity distributions evaluated at common value  $Q^2 = 3 \text{ (GeV/c)}^2$  as a function of  $x$  for two sets of fragmentation functions (DSS and EMC). Bands at bottom of graphs represent systematic uncertainties. Solid markers and bands correspond to PDFs obtained with DSS parameterisation of FFs. Open markers and bands are obtained with EMC parameterisation of FFs. The curves represent the LO DNS parameterisation of polarised PDFs [26].

to the assumptions generally made to reduce the number of FFs, the EMC analysis also assumed that  $D_s^{K^+} = D_u^{\pi^+}$ .

The recent HKNS parameterisation of FFs [23] strongly disagrees with the ratio of negative to positive hadrons observed in our data, as was already observed in [3] for the KRE parameterisation [24]. For this reason, these parameterisations based only on  $e^+e^-$  collider data are not usable in the kinematic range of the present analysis.

Since the analysis is based on deuteron data only, only the sums of  $u$  and  $d$  densities can be extracted:  $\Delta u_v + \Delta d_v$  and  $\Delta \bar{u} + \Delta \bar{d}$ . In principle  $\Delta s$  and  $\Delta \bar{s}$  could both be extracted from the charged kaon asymmetries  $A_{1,d}^{K^+}$  and  $A_{1,d}^{K^-}$  but in view of the precision of the data, they are assumed to be equal. All asymmetries are also assumed to be independent of  $Q^2$ . In this way the resulting PDFs are obtained at a common  $Q^2$  fixed to  $3 \text{ (GeV/c)}^2$ .

The five measured asymmetries form a linear system of equations with three unknowns ( $\Delta u_v + \Delta d_v$ ,  $\Delta \bar{u} + \Delta \bar{d}$ ,  $\Delta s$ ), which is solved by a least-square fit independently in each  $x$ -bin. Only statistical errors are used in the fit and correlations between asymmetries are taken into account. Two corrections ( $c_1, c_2$ ) are applied in the evaluation of quark helicity distributions from the asymmetries. The first one,  $c_1 = 1 - 1.5\omega_D$ , accounts for the deuteron D-state contribution ( $\omega_D = 0.05 \pm 0.01$  [25]). The second one accounts for the fact that, although  $R(x, Q^2) = 0$  at LO, the unpolarised PDFs originate from  $F_2$  distributions in which  $R = \sigma_L/\sigma_T$  was different from zero [19]. In the present analysis we assume  $R$  to be the same for inclusive and semi-inclusive reactions, so that the same correction,  $c_2 = 1 + R(x, Q^2)$ , can be used for inclusive and hadron asymmetries. The resulting quark helicities thus are corrected by a factor  $\xi = c_1 \cdot c_2$ .



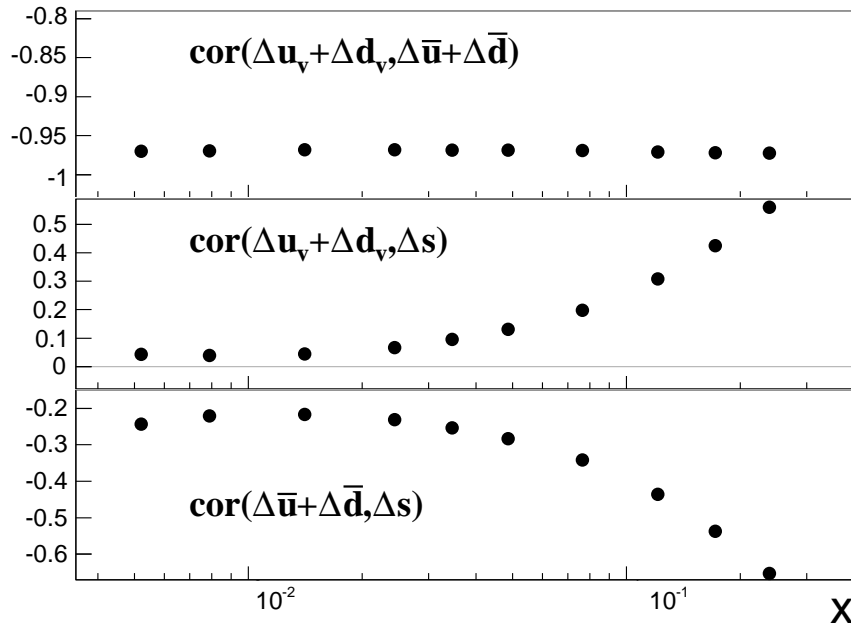


Figure 5: Correlation coefficients of PDFs obtained in the fit with DSS parameterisation as a function of  $x$ .

Table 1: First moments  $\Delta u_v + \Delta d_v$ ,  $\Delta \bar{u} + \Delta \bar{d}$  and  $\Delta s$  at  $Q^2 = 3 (\text{GeV}/c)^2$  from the COMPASS data and also from the DNS fit at LO [26] truncated to the range of the measurements ( $0.004 < x < 0.3$ ).

FF		DSS	EMC
$\Delta u_v + \Delta d_v$	measur.	$0.26 \pm 0.06 \pm 0.02$	$0.30 \pm 0.08 \pm 0.02$
	DNS	0.225	
$\Delta \bar{u} + \Delta \bar{d}$	measur.	$-0.04 \pm 0.03 \pm 0.01$	$-0.05 \pm 0.04 \pm 0.01$
	DNS	-0.009	
$\Delta s (= \Delta \bar{s})$	measur.	$-0.01 \pm 0.01 \pm 0.02$	$-0.05 \pm 0.03 \pm 0.03$
	DNS	-0.035	

The results of the fit obtained with the two sets of fragmentation functions are shown in Fig. 4. Significant differences are observed only for  $\Delta s$ . Indeed the main difference of DSS with respect to EMC is the enhanced  $s(\bar{s})$  quark contribution to the production of  $K^- (K^+)$ : the ratio  $\int_{0.2}^1 D_s^{K^+}(z) dz / \int_{0.2}^1 D_u^{K^+}(z) dz$ , which is equal to 3.4 for the quoted EMC values, increases to 6.6 in DSS. The statistical precision of  $\Delta s$  for the two parameterisations changes in the same proportion. The curves obtained with the LO DNS parameterisation of polarised PDFs [26] are also shown. As in our previous publication on the asymmetry of unidentified hadrons [3], a nice agreement is observed in the valence sector. The asymmetries of the non-strange sea are also compatible with the DNS curve, although we observe a tendency for the data points to be above and below the curve at low and high  $x$ , respectively. The shape of the  $x\Delta s$  curve of DNS is quite typical for QCD fits of  $g_1(x, Q^2)$  data, showing a minimum in the medium  $x$  region ( $x \approx 0.2$ ). With the DSS fragmentation functions, the SIDIS measurements of COMPASS do not seem to support this behaviour, while with the EMC ones, the errors become too large to draw any conclusion.

The elements of the correlation matrix for the obtained densities are shown in Fig. 5. The correlation between the non-strange densities  $\Delta u_v + \Delta d_v$  and  $\Delta \bar{u} + \Delta \bar{d}$  is large and negative. This feature can be explained by the fact that their sum is highly constrained by the very precise value of  $A_{1,d}$ : since the term with  $\Delta s$  in Eq. (2) is smaller than the other ones,  $A_{1,d}$  fixes well the sum of non-strange densities and forces them to anti-correlate.

The estimates of the truncated first moments  $\Delta u_v + \Delta d_v$ ,  $\Delta \bar{u} + \Delta \bar{d}$  and  $\Delta s$  are given in Table 1. The systematic errors have been estimated by refitting the asymmetries shifted simultaneously within the limits of their systematic uncertainty. The value quoted for valence quarks is in good agreement with the one derived in our previous publication from the difference asymmetries for non-identified hadrons obtained from a partially overlapping data sample ( $0.26 \pm 0.07 \pm 0.04$  at  $Q^2 = 10 (\text{GeV}/c)^2$ ) [3].

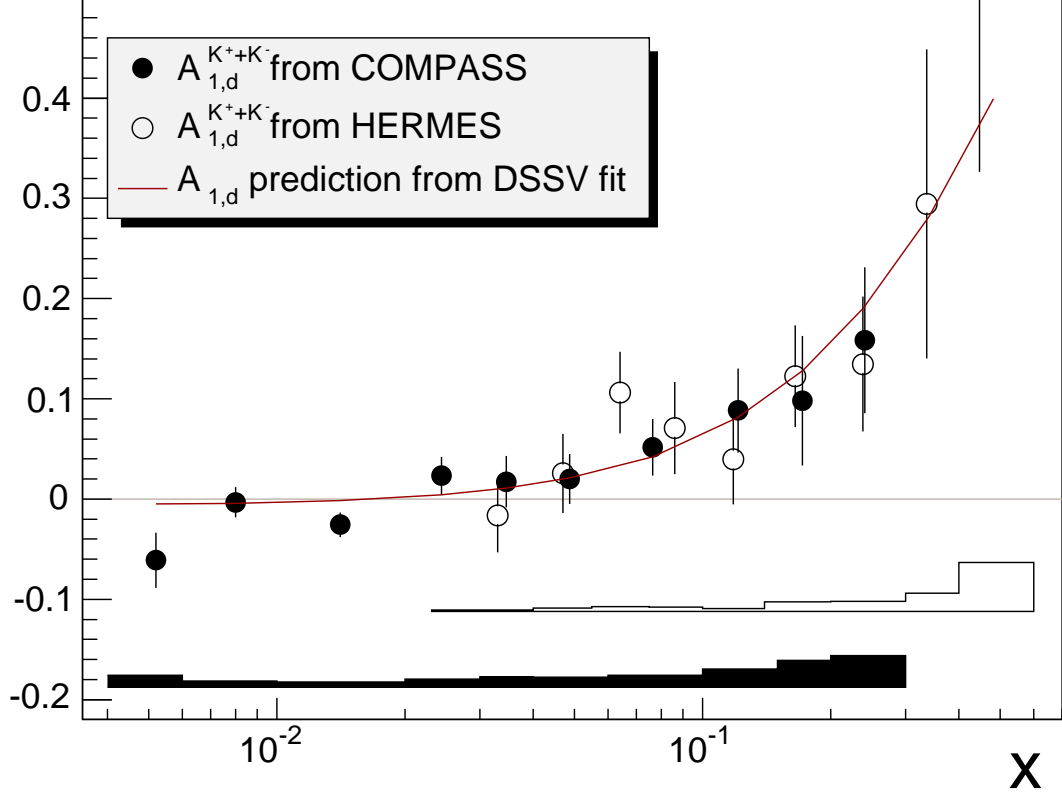


Figure 6: Charged kaon asymmetries obtained with cross-section weights from MRST PDFs and DSS FFs. For comparison results of HERMES [7] are also presented. The curve shows the  $A_{1,d}$  prediction of the DSSV fit [10].

### 5 Direct evaluation of $\Delta s$ from the charged kaon asymmetry

The dependence of  $\Delta s(x)$  on the FFs can be further explored in relation with the charged kaon asymmetry  $A_{1,d}^{K^++K^-}$ . This asymmetry is a weighted average of  $A_{1,d}^{K^+}$  and  $A_{1,d}^{K^-}$  with weights given by the spin-averaged  $K^+$  and  $K^-$  cross-sections

$$A_{1,d}^{K^++K^-} = \frac{\sigma^{K^+} A_{1,d}^{K^+} + \sigma^{K^-} A_{1,d}^{K^-}}{\sigma^{K^+} + \sigma^{K^-}}. \quad (3)$$

It is found to be very stable with respect to the ratio  $\sigma^{K^-}/\sigma^{K^+}$ . Indeed a change of this ratio by  $\pm 10\%$  does not modify  $A_{1,d}^{K^++K^-}$  by more than 10% of its statistical error. At LO, the cross-section ratio only depends on the unpolarised PDFs and on the ratios of unfavoured to favoured and strange to favoured FFs:

$$R_{UF} = \frac{\int D_d^{K^+}(z) dz}{\int D_u^{K^+}(z) dz}, \quad R_{SF} = \frac{\int D_s^{K^+}(z) dz}{\int D_u^{K^+}(z) dz} \quad (4)$$

which are respectively equal to 0.13 and 6.6 for the DSS FFs at  $Q^2 = 3 \text{ (GeV}/c)^2$  (0.35 and 3.4 for the EMC FFs).<sup>2)</sup> The values shown in Fig. 6 have been obtained with the MRST PDFs and the DSS FFs. As for the  $K^+$  and  $K^-$  asymmetries, they are in very good agreement with the HERMES values of Ref. [7].

For an isoscalar target, the charged kaon asymmetry and the inclusive asymmetry can be written at LO as

$$A_{1,d}^{K^++K^-} = \xi \frac{\Delta Q + \alpha \Delta s}{Q + \alpha s}, \quad A_{1,d} = \xi \frac{\Delta Q + \frac{4}{5} \Delta s}{Q + \frac{4}{5} s} \quad (5)$$

where  $Q$  is the non-strange quarks density  $Q = u + \bar{u} + d + \bar{d}$ , the corresponding helicity density is  $\Delta Q$ , and  $\alpha = (2R_{UF} + 2R_{SF})/(2 + 3R_{UF})$ .

<sup>2)</sup> These values remain practically unchanged when the range of  $z$  is limited to 0.85 instead of 1.

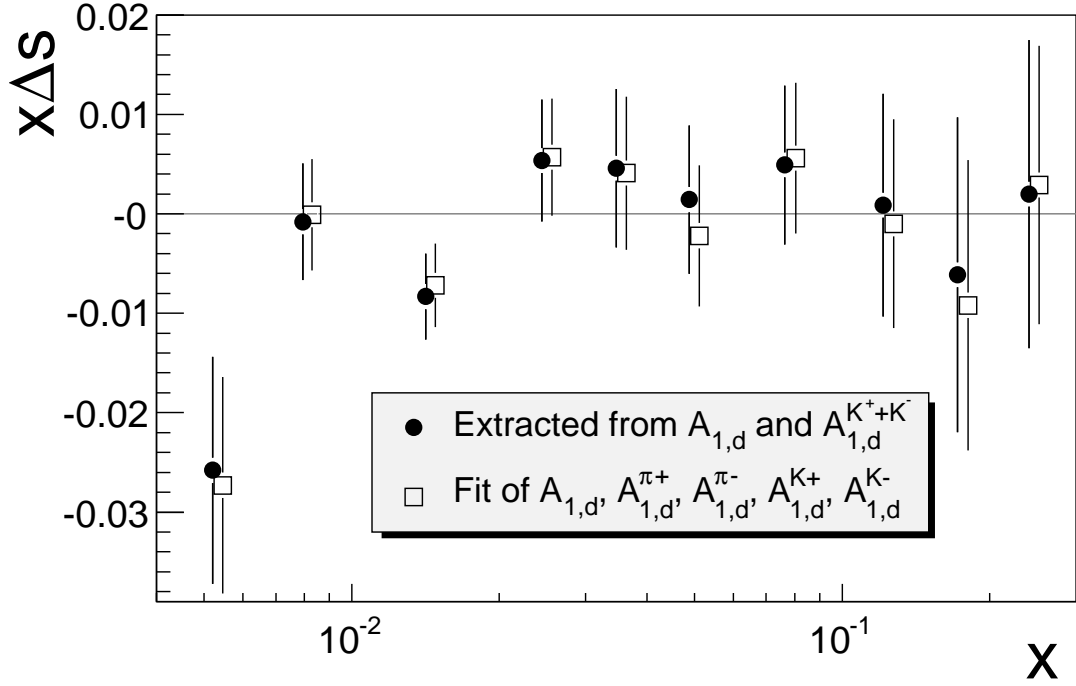


Figure 7: The strange quark spin distribution  $x \Delta s(x)$  at  $Q^2 = 3 (\text{GeV}/c)^2$  derived from the charged kaon asymmetry  $A_{1,d}^{K^+K^-}$  using DSS FFs and from  $A_{1,d}$ , compared to the result of the corresponding least square fit. The quoted errors are statistical only.

To take advantage of the similarity between  $A_{1,d}^{K^+K^-}$  and  $A_{1,d}$ , it is convenient to write the strange quark polarisation  $\Delta s/s$  in the form

$$\frac{\Delta s}{s} = \frac{1}{\xi} \left[ A_{1,d} + (A_{1,d}^{K^+K^-} - A_{1,d}) \frac{Q/s + \alpha}{\alpha - 0.8} \right], \quad (6)$$

where  $Q$  and  $s$  are spin-independent non-strange and strange quark densities. As expected, the use of this formula leads to values of  $\Delta s$  practically equal to those of the least square fit but with slightly larger statistical errors (Fig. 7). The above formula shows that in the special case where  $A_{1,d}^{K^+K^-}$  would be strictly equal to  $A_{1,d}$ , the strange quark helicity would become insensitive to FFs and its first moment would be small and positive ( $\approx 0.006$ ). Otherwise the main dependence on the FFs is due to  $R_{SF}$ , which appears only in the numerator of  $\alpha$ , and its effect is amplified by the large values of the ratio  $Q/s$ . Negative values of  $\Delta s$  correspond to negative values of  $A_{1,d}^{K^+K^-}$  at low  $x$  where  $A_{1,d}^d \approx 0$  and to  $A_{1,d}^{K^+K^-} < A_{1,d}$  at higher  $x$ . The  $A_{1,d}(x)$  prediction of the DSSV fit [10] is shown in Fig. 6 for comparison. Neither the COMPASS nor the HERMES points show any tendency to lie below the  $A_{1,d}$  curve in the range  $0.03 < x < 0.3$ . There is thus no indication for a significantly negative  $\Delta s$  in this region, in contrast to predictions of most fits using only  $g_1$  data, as shown for instance by the DNS prediction in Fig. 4. The COMPASS values of  $A_{1,d}^{K^+K^-}$  provide at least a hint that  $\Delta s$  may become negative in the previously unmeasured low  $x$  region ( $x < 0.02$ ), as predicted in the recent DSSV fit [10].

Fig. 8 shows the variation of the first moment of  $\Delta s$  truncated to the measured region as a function of  $R_{SF}$ . For  $R_{SF} \gtrsim 5$ , we observe that the values are close to zero and larger than the full moment derived from the inclusive analysis (Eq. 1). The contribution from the region  $x > 0.3$  is limited by the positivity condition  $|\Delta s(x)| \leq s(x)$  and cannot exceed 0.003 in absolute value. Thus any difference between the truncated SIDIS moment and the full moment must be compensated by an unmeasured contribution in the low  $x$  region. In particular this is the case for the DSS FFs where  $R_{SF} = 6.6$ . The difference never exceeds two standard deviations, so that no firm conclusions can be drawn from the COMPASS data only, nevertheless, as shown on Fig. 6, the HERMES data lead to a similar result. In contrast, if  $R_{SF} \lesssim 4$ , the asymmetry  $A_{1,d}^{K^+K^-}$  becomes less and less sensitive to  $\Delta s$  because  $D_s^{K^+}$  is small. This is the case for the EMC FFs and, in general, for older parameterisations such as KRE [24].

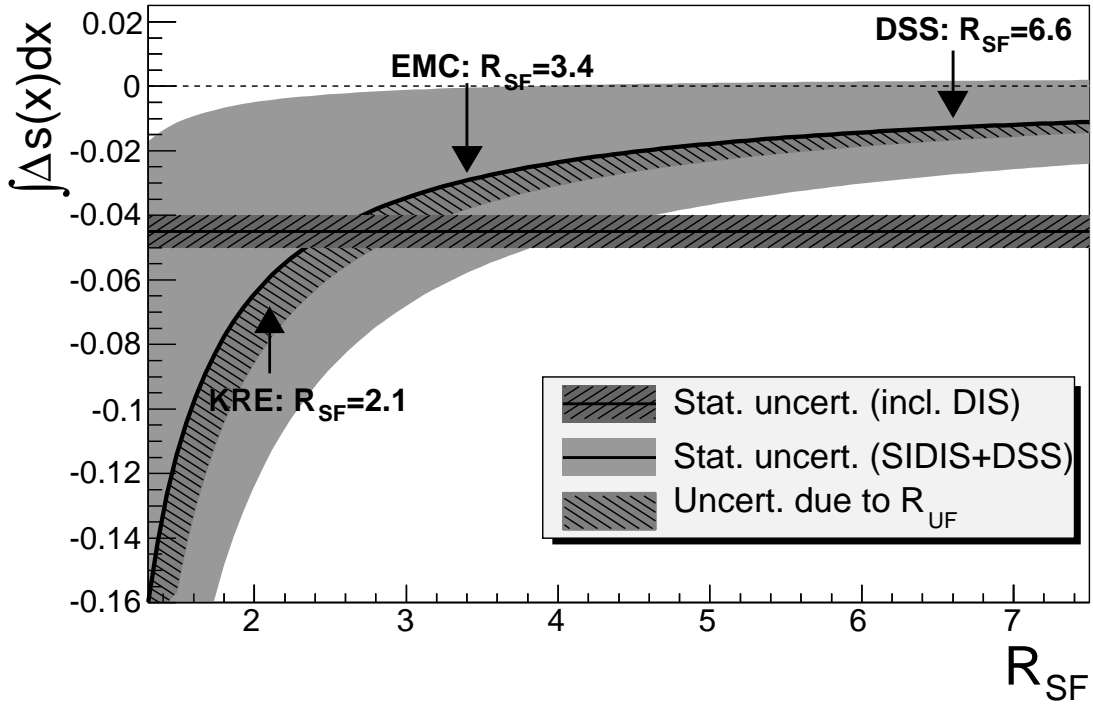


Figure 8: Integral of  $\Delta s$  over the measured range of  $x$ , as a function of the ratio  $R_{SF}$  for  $R_{UF}$  fixed at the DSS value of 0.13 (thick solid curve). The light-grey area shows the statistical uncertainty and the hatched band inside of it shows the effect of increasing  $R_{UF}$  to 0.35 (EMC value). The horizontal band represents the full moment of  $\Delta s$  derived from the COMPASS value of the first moment of  $g_1^d(x)$  (Eq. 1). The values of  $R_{SF}$  corresponding to DSS[21], EMC[22] and KRE[24] parameterisations of FFs are indicated by arrows.

## 6 Conclusions

We have presented a first measurement of the longitudinal spin asymmetries for charged pions and kaons identified with the RICH detector in the COMPASS experiment. These measurements are used in combination with the inclusive asymmetries to evaluate the polarised valence, non-strange sea and strange quark distributions. The results for valence quarks and non-strange sea quarks are in good agreement with the DNS parameterisation. They show weak dependence on the selected parameterisation of the fragmentation functions. The distribution of  $\Delta s$  is compatible with zero in the whole measured range, in contrast to the shape of the strange quark helicity distribution obtained in most LO and NLO QCD fits. The value of the first moment of  $\Delta s$  and its error are very sensitive to the assumed value of the ratio of the  $\bar{s}$ -quark to  $u$ -quark fragmentation functions into positive kaons  $\int D_s^{K^+}(z)dz / \int D_u^{K^+}(z)dz$ .

## Acknowledgements

We gratefully acknowledge the support of the CERN management and staff and the skill and effort of the technicians of our collaborating institutes. Special thanks go to V. Anosov and V. Pesaro for their technical support during the installation and the running of this experiment. This work was made possible thanks to the financial support of our funding agencies.

## References

- [1] EMC, J. Ashman *et al.*, Phys. Lett. B 206 (1988) 364.
- [2] HERMES Collaboration, A. Airapetian *et al.*, Phys. Rev. D 75 (2007) 012007.
- [3] COMPASS Collaboration, M. Alekseev, *et al.*, Phys. Lett. B 660 (2008) 458.
- [4] COMPASS Collaboration, V.Yu. Alexakhin *et al.*, Phys. Lett. B 647 (2007) 8.
- [5] E. Leader, A.V. Sidorov, D.B. Stamenov, Phys. Rev. D 75 (2007) 074027.
- [6] HERMES Collaboration, A. Airapetian *et al.*, Phys. Rev. Lett. 92 (2004) 012005.
- [7] HERMES Collaboration, A. Airapetian *et al.*, Phys. Rev. D 71 (2005) 012003.
- [8] HERMES Collaboration, A. Airapetian *et al.*, Phys. Lett. B 666 (2008) 446.
- [9] E. Leader, D.B. Stamenov, Phys. Rev. D 67 (2003) 037503.
- [10] D. de Florian, R. Sassot, M. Stratmann, W. Vogelsang, Phys. Rev. Lett. 101 (2008) 072001.

Table 2: Values of the inclusive asymmetry  $A_{1,d}$  with their statistical and systematic errors as a function of  $x$ , with the corresponding average value of  $Q^2$ .

$x$ -bin	$\langle x \rangle$	$\langle Q^2 \rangle$ (GeV/c) $^2$	$A_{1,d} \pm \delta A_{stat} \pm \delta A_{syst}$
0.004–0.006	0.0052	1.17	$0.001 \pm 0.005 \pm 0.002$
0.006–0.010	0.0079	1.48	$-0.001 \pm 0.003 \pm 0.001$
0.010–0.020	0.0141	2.15	$-0.002 \pm 0.003 \pm 0.001$
0.020–0.030	0.0244	3.23	$0.010 \pm 0.005 \pm 0.002$
0.030–0.040	0.0346	4.33	$0.003 \pm 0.006 \pm 0.003$
0.040–0.060	0.0487	5.87	$0.016 \pm 0.006 \pm 0.003$
0.060–0.100	0.0765	8.63	$0.039 \pm 0.007 \pm 0.004$
0.100–0.150	0.121	12.9	$0.090 \pm 0.010 \pm 0.008$
0.150–0.200	0.172	17.8	$0.126 \pm 0.015 \pm 0.011$
0.200–0.300	0.240	24.9	$0.159 \pm 0.017 \pm 0.014$

- [11] SMC, B. Adeva *et al.*, Phys. Lett. B 420 (1998) 180.
- [12] COMPASS Collaboration, P. Abbon *et al.*, Nucl. Instr. Meth. A 577 (2007) 455.
- [13] D. Adams *et al.*, Nucl. Instrum. Meth. A 437 (1999) 23.
- [14] N. Doshita *et al.*, AIP Conf. Proc. 980 (2008) 307; F. Gautheron, AIP Conf. Proc. 915 (2007) 961.
- [15] J. Ball *et al.*, Nucl. Instrum. Meth. A 498 (2003) 101.
- [16] P. Abbon *et al.*, Eur. Phys. J.ST 162 (2008) 251; P. Abbon *et al.*, Nucl. Instrum. Meth. A 595 (2008) 23.
- [17] V. Aleksakhin, Y. Bedfer, S. Gerasimov, A. Korzenev, Phys. Part. Nucl. Lett. 4 (2007) 350.
- [18] I.V. Akushevich, N.M. Shumeiko, J. Phys. G 20 (1994) 513.
- [19] E143 Collaboration, K. Abe *et al.*, Phys. Lett. B 452 (1999) 194.
- [20] A.D. Martin, W.J. Stirling, R.S. Thorne, Phys. Lett. B 636 (2006) 259.
- [21] D. de Florian, R.Sassot, M. Stratmann, Phys. Rev. D 75 (2007) 114010.
- [22] EMC, A. Arneodo *et al.*, Nucl. Phys. B 321 (1989) 541.
- [23] M. Hirai, S. Kumano, T.-H. Nagai, K. Sudoh, Phys. Rev. D 75 (2007) 094009.
- [24] S. Kretzer, Phys. Rev. D 62 (2000) 054001.
- [25] R. Machleidt *et al.*, Phys. Rep. 149 (1987) 1.
- [26] D. de Florian, G.A. Navarro, R. Sassot, Phys. Rev. D 71 (2005) 094018.

Table 3: Unfolded hadron asymmetries of charged pions and kaons.

$\langle x \rangle$	$\langle Q^2 \rangle$ (GeV/c) <sup>2</sup>	$A_{1,d}^{\pi^+} \pm \delta A_{stat}^{\pi^+} \pm \delta A_{syst}^{\pi^+}$	$A_{1,d}^{\pi^-} \pm \delta A_{stat}^{\pi^-} \pm \delta A_{syst}^{\pi^-}$	$A_{1,d}^{K^+} \pm \delta A_{stat}^{K^+} \pm \delta A_{syst}^{K^+}$	$A_{1,d}^{K^-} \pm \delta A_{stat}^{K^-} \pm \delta A_{syst}^{K^-}$
0.0052	1.16	0.006 ± 0.014 ± 0.006	0.009 ± 0.014 ± 0.006	-0.018 ± 0.029 ± 0.011	-0.084 ± 0.030 ± 0.014
0.0079	1.42	-0.003 ± 0.008 ± 0.003	-0.002 ± 0.008 ± 0.003	-0.017 ± 0.017 ± 0.007	0.014 ± 0.018 ± 0.007
0.0141	2.03	-0.003 ± 0.007 ± 0.003	-0.007 ± 0.007 ± 0.003	-0.039 ± 0.014 ± 0.006	-0.004 ± 0.016 ± 0.006
0.0244	3.19	-0.001 ± 0.011 ± 0.004	0.006 ± 0.012 ± 0.005	0.020 ± 0.022 ± 0.009	0.025 ± 0.026 ± 0.010
0.0346	4.43	0.026 ± 0.015 ± 0.006	0.004 ± 0.016 ± 0.006	0.021 ± 0.030 ± 0.012	0.012 ± 0.035 ± 0.014
0.0487	6.10	0.016 ± 0.015 ± 0.006	0.037 ± 0.016 ± 0.007	0.066 ± 0.029 ± 0.011	-0.058 ± 0.035 ± 0.015
0.0763	9.26	0.046 ± 0.017 ± 0.008	0.018 ± 0.018 ± 0.007	0.064 ± 0.032 ± 0.013	0.015 ± 0.041 ± 0.017
0.121	14.9	0.094 ± 0.025 ± 0.012	0.087 ± 0.028 ± 0.013	0.117 ± 0.046 ± 0.019	-0.007 ± 0.065 ± 0.026
0.171	22.4	0.102 ± 0.039 ± 0.017	0.132 ± 0.044 ± 0.020	0.116 ± 0.070 ± 0.028	0.002 ± 0.103 ± 0.041
0.240	32.8	0.218 ± 0.044 ± 0.024	0.147 ± 0.051 ± 0.023	0.208 ± 0.078 ± 0.031	-0.018 ± 0.118 ± 0.047

Table 4: Correlation coefficients of unfolded asymmetries in bins of  $x$ .

$x$ -bin	0.004-0.006	0.006-0.01	0.01-0.02	0.02-0.03	0.03-0.04	0.04-0.06	0.06-0.10	0.10-0.15	0.15-0.20	0.20-0.30
$A_{1,d}^{\pi^+} \& A_{1,d}$	0.29	0.34	0.39	0.40	0.40	0.41	0.41	0.40	0.39	0.39
$A_{1,d}^{\pi^-} \& A_{1,d}$	0.30	0.35	0.38	0.39	0.39	0.39	0.38	0.36	0.35	0.34
$A_{1,d}^{\pi^-} \& A_{1,d}^{\pi^+}$	0.12	0.15	0.17	0.16	0.16	0.16	0.16	0.15	0.15	0.17
$A_{1,d}^{K^+} \& A_{1,d}$	0.11	0.15	0.17	0.19	0.19	0.20	0.21	0.21	0.21	0.21
$A_{1,d}^{K^+} \& A_{1,d}^{\pi^+}$	-0.18	-0.12	-0.08	-0.06	-0.05	-0.04	-0.04	-0.03	-0.02	-0.02
$A_{1,d}^{K^+} \& A_{1,d}^{\pi^-}$	0.03	0.04	0.04	0.04	0.04	0.04	0.04	0.05	0.05	0.05
$A_{1,d}^{K^-} \& A_{1,d}$	0.11	0.14	0.16	0.16	0.16	0.16	0.16	0.15	0.14	0.14
$A_{1,d}^{K^-} \& A_{1,d}^{\pi^+}$	0.03	0.03	0.03	0.03	0.03	0.03	0.03	0.03	0.03	0.03
$A_{1,d}^{K^-} \& A_{1,d}^{\pi^-}$	-0.14	-0.09	-0.05	-0.04	-0.04	-0.03	-0.03	-0.03	-0.03	-0.04
$A_{1,d}^{K^-} \& A_{1,d}^{K^+}$	0.05	0.07	0.09	0.10	0.10	0.10	0.10	0.10	0.11	0.12